Organic Electronics 13 (2012) 1315–1321

Contents lists available at SciVerse ScienceDirect

Organic Electronics

journal homepage: www.elsevier.com/locate/orgel

Nano-morphology characterization of organic bulk heterojunctions based on mono and bis-adduct fullerenes

Hamed Azimi [a,c,*], Darcy Fournier [b], Maarten Wirix [d], Edmund Dobrocka [e], Tayebeh Ameri [g], Florian Machui [g], Sheila Rodman [b], Gilles Dennler [b], Markus C. Scharber [a], Kurt Hingerl [c], Joachim Loos [f], Christoph J. Brabec [g], Mauro Morana [a]

[a] Konarka Austria, Altenbergerstrasse 69, A-4040 Linz, Austria
[b] Konarka Technologies Inc. Boott Mill South, 116 John Street, Suite 12, Lowell, MA 01852, USA
[c] Christian Doppler Laboratory for Surface Optics, Johannes Kepler University, A-4040 Linz, Austria
[d] Laboratory of Materials and Interface Chemistry and Soft Matter CryoTEM Research Unit, Eindhoven University of Technology, PO Box 513, NL-5600 MB Eindhoven, The Netherlands
[e] Institute of Electrical Engineering, SAS, Dúbravská cesta 9, 841 04 Bratislava, Slovakia
[f] School of Physics and Astronomy, Kelvin Nanocharacterisation Centre, University of Glasgow, Glasgow G12 8QQ, Scotland, UK
[g] Friedrich-Alexander-University, Martensstraße 7, 91058 Erlangen, Germany

ARTICLE INFO

Article history:
Received 16 January 2012
Received in revised form 21 February 2012
Accepted 23 March 2012
Available online 7 April 2012

Keywords:
Organic photovoltaic
PCBM
Bis-PCBM
Crystallinity
Morphology

ABSTRACT

We have studied organic bulk heterojunction photovoltaic devices based on a bridged-bithiophene donor–acceptor type low-band gap polymer blended with PCBM and bis-PCBM. The impact of the molecular arrangement is discussed in terms of the correlation between the solar-cell performance and the degree of crystallization. Differential scanning calorimetry (DSC) and grazing-incidence X-ray diffraction (GIXRD) prove that films with bis-PCBM typically result in more amorphous blends than comparable films with PCBM. Electron tomography (ET) is used to visualize the three dimensional morphology of photo-active layers, confirming the presence of nanofibers, formed in different scales through the thickness in the blended films with mono and bis-fullerenes.

1. Introduction

A tremendous effort was made towards improving the performance of organic photovoltaics (OPVs) by implementing novel acceptors over the past few years [1–7]. Within the compass of these appreciable amount of studies, the need for studying morphological features of the new acceptors and particularly their interaction with the donor compound became far more demanding. Fullerenes, which are among the best sensitizers for photorefractive polymers and possessing a variety of lowest unoccupied molecular orbital (LUMO) levels, are now in the focus for organic photovoltaic applications. Attempts to raise the open circuit voltage (V_{oc}) of OPVs by reducing the LUMO–LUMO offset of polymer and fullerene by investigations on the C_{60} and C_{70} fullerene derivatives, especially the dyads and triads (bis and tris), spurred the efficiency of organic PVs to more promising values [8,9]. However, it is still an open question to what degree raising the acceptor LUMO level changes the photoinduced charge transfer process with the polymer. The blend of poly(3-hexylthiophene) (P3HT) and bis-adduct of [6,6]-phenyl-C_{61}-butyric acid methyl ester (bis-PCBM) is one of the rare systems that demonstrates an improvement in power conversion efficiency (PCE) over the mono-adduct (PCBM) [9]. In this case, the modest reduction in donor/acceptor LUMOs offset of about 100 meV appears to have no significant impact on the charge transfer between the

* Corresponding author. Present address: Friedrich-Alexander-University, Martensstraße 7, 91058 Erlangen, Germany. Tel.: +43 732 2468 5120; fax: +43 732 2468 5119.
E-mail address: hamed.azimi@ww.uni-erlangen.de (H. Azimi).

1566-1199/$ - see front matter © 2012 Elsevier B.V. All rights reserved.
http://dx.doi.org/10.1016/j.orgel.2012.03.031

two species. The lower photocurrent of the system containing bis-adduct has been instead assigned to the non-ideal morphology and the microstructural discrepancies with mono-adducts [10]. In addition, Lenes et al. pointed out the importance of a reduced electron transport in fullerene multiadducts due to possible shallow traps in these systems [11]. The multiplicity of different isomers was suggested as the main cause for low electron mobility. Apart from the investigations with P3HT, little attention has been paid to the use of bis-fullerenes in combination with other higher performance polymers. One of these polymers is poly[2,6-(4,4-bis-(2-ethylhexyl)-4H-cyclopenta[2,1-b;3,4-b']-dithiophene)-alt-4,7-(2,1,3-benzothiadiazole)] (PCPDTBT), which has a band gap of 1.46 eV and can deliver efficiencies in the range of 5% [12]. Substitution of a carbon atom on the methylene bridge of the bithiophene unit with a silicon atom yields the polymer Si-PCPDTBT (poly[(4,4′-bis(2-ethylhexyl)dithieno[3,2-b:2′,3′-d]silole)-2,6-diyl-alt-(4,7-bis(2-thienyl)-2,1,3-benzothiadiazole)-5,5′-diyl]). Si-PCPDTBT is more crystalline than PCPDTBT, has superior charge carrier mobility and has low bimolecular recombination losses when blended with PCBM [13,14]. It is shown that the morphological evolution and higher crystallinity in Si-PCPDTBT:PCBM blends resulted from a more favorable domain size of the donor–acceptor phase which appeared in a way related to the inactivation of a charge transfer complex without any need of additives like 1,8-octanedithiol (ODT) [15]. Achieving a higher V_{oc} and an acceptable photocurrent density by using bis-adducts is therefore a desirable concomitant for such low band gap polymers.

Here, we have studied the bulk heterojunction (BHJ) solar cells made from the blends of Si-PCPDTBT with mono and bis-fullerene. It is shown that using bis-PCBM instead of mono-PCBM considerably increases the recombination losses and as a result deteriorates the device performance [16,17]. Our findings show that the major losses arise from a change in the microstructure rather than from the reduction of the offset between the lowest unoccupied molecular orbitals of the donor and the acceptor. The low charge carrier mobilities measured for Si-PCPDTBT:bis-PCBM was found to be a key factor in enhancing the charge carrier recombination [17]. Here, we present morphological results that translate the worse transport properties of the bis-PCBM solar cells to an unfavorable microstructure. Conventional differential scanning calorimetry (DSC) and modulated temperature DSC (MTDSC) were used to study the physical properties of PCBM and bis-PCBM. The structural properties of photoactive layers were characterized by using grazing-incidence X-ray diffraction (GIXRD). An overview on the organization in the nm regime is given by reconstructing the three-dimensional (3D) morphology via electron tomography (ET) imaging.

2. Experimental

The preparation of poly[(4,4′-bis(2-ethylhexyl)dithieno[3,2-b:2′,3′-d]silole)-2,6-diyl-alt-(4,7-bis(2-thienyl)-2,1,3-benzothiadiazole)-5,5′-diyl](Si-PCPDTBT, Mw 30–40 kDa) has been described in a patent [18]. The organic BHJ photovoltaic devices were fabricated on indium tin oxide (ITO) coated glass substrates. Devices were produced with the following layer sequence: indium tin oxide (ITO)/poly(3,4-ethylenedioxythiophene doped with polylstyrene sulfonate) (PEDOT:PSS)/active layer/LiF/Al, details described in Refs. [19,20]. All the active layers were prepared from o-dichlorobenzene and coated by a doctor-blade technique at the substrate temperature of 80 °C for the devices comprised of Si-PCPDTBT and 65 °C for the P3HT based devices. The fullerene concentration of 60 wt% was used for producing the Si-PCPDTBT devices and 50 wt% fullerene concentration for the P3HT devices. The thickness of Si-PCPDTBT:fullerene and P3HT:fullerene photoactive layers in solar cell structure were about 100 nm. P3HT devices were annealed at 140 °C for 5 min. The current–density–voltage characteristics of the devices were measured under illumination of AM1.5 (100 mW cm^{-2}) using a source measurement unit SMU 2400 from Keithley under nitrogen atmosphere.

All DSC and MTDSC measurements were performed on a TA Instruments DSC Q200 equipped with a Refrigerated Cooling System (RCS). Samples were prepared by packing about 11 mg of fullerene powder (Solenne) into a DSC Tzero pan. The pan was hermetically sealed with a small hole punched into the top of the lid.

XRD analysis was carried out using Bruker D8 DISCOVER diffractometer equipped with X-ray tube with rotating Cu anode operating at 12 kW and a wavelength of 0.154 nm. All measurements were performed in parallel beam geometry with parabolic Goebel mirror in the primary beam. The X-ray diffraction patterns were measured in grazing incidence set-up with the angle of incidence 1.5°. The scattering plane was perpendicular to the sample surface. The primary beam was limited to 0.2 mm width. At these conditions the irradiated area was 7.6 mm wide. The crystallite size analyses are performed based on the Scherrer's approach [21]. In the process of crystallite size determination the effect of the measuring geometry on the line broadening has been taken into account via the instrumental function of the diffractometer. All films were made by dissolving the polymers and PCBM or bis-PCBM in o-dichlorobenzene at a 3% (w/w) ratio. Films were doctor bladed on quartz substrates that gave a low background signal in the XRD measurements. For these measurements, the thickness of pristine fullerenes and polymer films was about 250–300 nm and the thickness of P3HT:fullerene and Si-PCPDTBT:fullerene blend films was approximately 400 nm and 700 nm, respectively. Samples comprising P3HT were annealed inside the glovebox at 140 °C for 5 min.

The Si-PCPDTBT:PCBM and Si-PCPDTBT:bis-PCBM layers for TEM and ET measurements were floated, by dissolving the water-soluble PEDOT:PSS layer and bringing the photoactive layer onto a surface of demineralized water, and picked up with 200-mesh copper TEM grids. The film compositions and preparations were consistent with those generally used in optimized solar cells. Bright-field TEM morphological observations and acquisition of tilt series for electron tomography were performed on a Technai G2 20 operated at 200 kV.

3. Results and discussion

3.1. Photovoltaic devices

Fig. 1a shows the current–density–voltage (J–V) characteristics of devices fabricated from mono and bis-PCBM blended with Si-PCPDTBT. Despite the 100 mV higher V_{oc} of Si-PCPDTBT:bis-PCBM devices, the lower fill factor (FF) and short circuit current density (J_{sc}) lead to an overall reduced efficiency of these devices. In contrast, P3HT:bis-PCBM devices show only a slight reduction in J_{sc}, no reduction in FF and at least a 150 mV increase in V_{oc} (Fig. 1b) resulting in an overall increased PCE as compared to PCBM.

3.2. DSC and MTDSC measurements

Calorimetric techniques are an efficient analytical tool to characterize the mixing properties of multicomponent systems. Differential scanning calorimetry (DSC) was recently successfully applied to investigate the phase diagram of polymer–fullerene blends [22–25]. Fig. 2 shows the heat flow (HF) trace curves of bis-PCBM measured by means of standard DSC. Three heat–cool cycles were run where the second and third cycles looked nearly identical. The first heat cycle shows transitions due to the thermal history of the sample and is not shown. The transition observed at 160 °C has the shape of a melting type transition. However, more careful analysis reveals this peak as a glass transition (T_g) obscured by enthalpic relaxation. When a glass transition is weak, and set against a rising baseline due to the gradual increase in heat capacity of other components, the presence of a relaxation endotherm can give the impression of an endothermic process rather than a glass transition In such a situation, thermally modulated DSC measurements can give the correct assignment by subtracting the unwanted background signals [26]. MTDSC was run on the same samples to bypass thermal history events. The sample was run at a rate of 2 °C/min from −40 °C to 250 °C using a modulation of ±1.00 °C/min every 60 s. Once the signals were separated, it is clear that the transition at 162 °C is a glass transition, as shown in the reversing HF signal in Fig. 3. A glass transition observed in the reversing signal provides the enthalpy change that appears in the non-reversing signal (the signal at 160 °C). For PCBM, the observation of a glass transition signal is only reported by few groups [27], however most studies observed melting peaks at about 285–295 °C [23,28,29] (see appendix our measurement, Fig. A.1). For the pure bis-PCBM, although we observe a T_g at 162 °C, but after this transition we could not detect any melting transitions up to 350 °C, at which point the sample begins to degrade (see appendix for the measurement above 300 °C, Fig. A.2). The absence of a crystallization exotherm after the T_g and melting transition for bis-PCBM, which is normally seen for PCBM, suggests a higher amorphous portion in bis-PCBM.

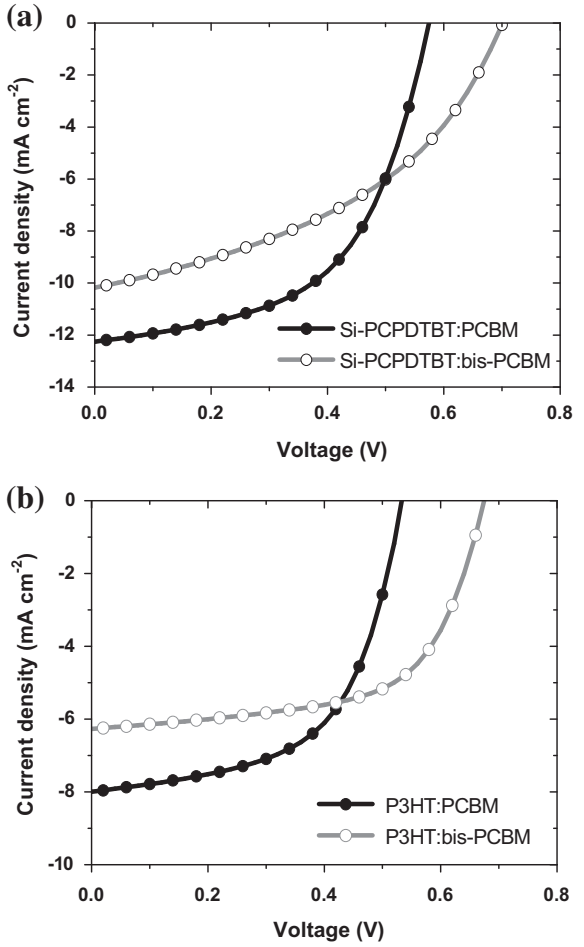

Fig. 1. J–V characteristics of solar cells comprising active layer of (a) Si-PCPDTBT:PCBM versus Si-PCPDTBT:bis-PCBM (b) P3HT:PCBM versus P3HT:bis-PCBM with a thickness of around 100 nm under simulated 1.5 AM illumination.

3.3. X-ray diffraction

GIXRD measurements were initially performed for pristine films of mono and bis-fullerene (Fig. 4). Two peaks

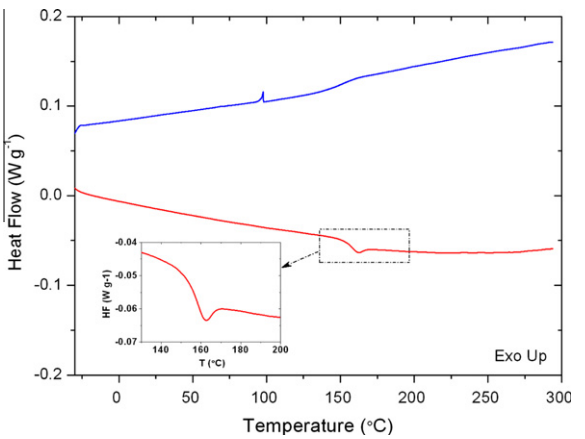

Fig. 2. DSC thermogram for the bis-PCBM powder at a heating/cooling rate of 5 °C/min; showing the second heating cycle (lower, red curve) and second cooling cycle (upper, blue curve). The peak in the cooling curve at 100 °C is an artifact. (For interpretation of the references to color in this figure legend, the reader is referred to the web version of this article.)

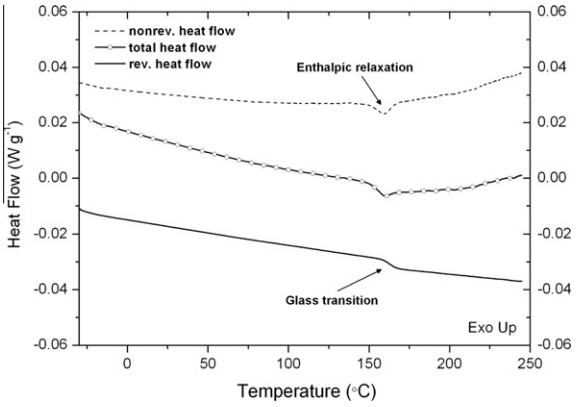

Fig. 3. Thermally-modulated DSC of bis-PCBM powder showing the total heat flow, reversing heat flow and non-reversing heat flow signals.

appear in the XRD spectra of neat fullerene films, one at $2\theta = 19.4°$ and a less intense one at 10°. Bis-PCBM shows one strong diffraction peak at 20° with the same broadening as PCBM, while the peak at 10° appears weaker (as the inset of Fig. 4 magnifies the corresponding peak), which may indicate a lower degree of ordering in bis-PCBM, given that both films have same thickness. This observation is also in line with the DSC measurements. Similar measurements were performed on Si-PCPDTBT and P3HT blended with mono and bis-fullerene. Fig. 5 shows the diffraction characteristics of pristine Si-PCPDTBT together with its blend with PCBM and bis-PCBM. The intense peak at $2\theta = 5.04°$ represents an *a*-axis distance of ca. 17.5 Å between the polymer backbones, separated via ethylhexyl groups. The weaker feature at 25.26° represents the π–π stacking between polymer chains along the *b*-axis [14,30]. The π–π stacking of Si-PCPDTBT is estimated at 3.5 Å, which is shorter than the value measured for P3HT. The diffraction peaks centered at 10° and 19.4° are evidently associated with the fullerene phase. The analysis of the diffraction peaks showed that the π–π stacking distance and the *a*-axis distance between the polymer chains

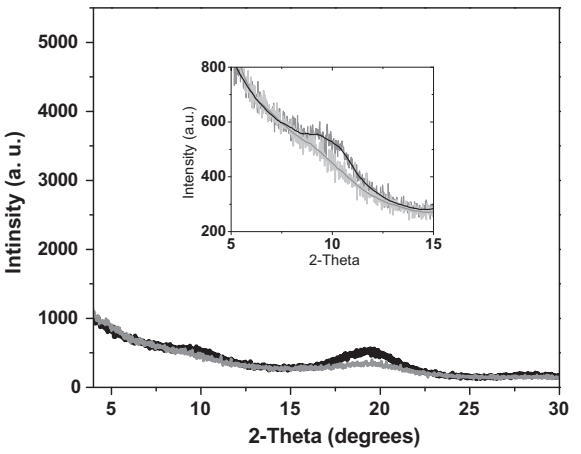

Fig. 4. GIXRD of films of pristine bis-PCBM, 250 nm thick (gray color) versus the pristine PCBM, 250 nm thick (black color) deposited on quartz substrates. The inset of graph zooms the peak at around $2\theta = 10°$.

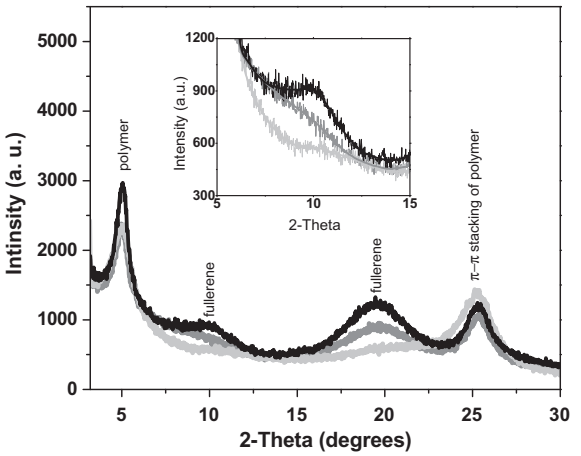

Fig. 5. GIXRD images of films of pristine Si-PCPDTBT (light gray), blend Si-PCPDTBT:bis-PCBM (dark gray) and Si-PCPDTBT:PCBM (black) deposited on quartz substrates.

is not changed by replacing PCBM with bis-PCBM. However, the signal attributed to the fullerene phase is different for Si-PCPDTBT:PCBM and Si-PCPDTBT:bis-PCBM films. This can be concluded from the suppression of the bis-PCBM peak at 19.45° and an even more incomplete appearance of the diffraction signal at 10°. In addition from the half width of peak at 17.5 Å, a minimum crystallite size of 16.2 nm is calculated along the *a*-axis direction of Si-PCPDTBT:PCBM. This is slightly larger than the 13.8 nm value found for Si-PCPDTBT:bis-PCBM. It is worth mentioning that in the GIXRD measurements, we generally study the crystalline parts of the samples. There are also indeed some amorphous polymer and fullerene regions that cannot be directly investigated here.

XRD measurements were also performed on P3HT:PCBM and P3HT:bis-PCBM for comparison. The diffraction spectra appear more or less identical (Fig. 6). The spacing between the main chains of P3HT was calculated with 16.5 Å and the π–π stacking of thiophene rings was measured with 3.8 Å. These distances agree with the values previously reported for P3HT [31,32]. In P3HT blend films, the weak diffraction of fullerene at 10° is no longer observed, and the diffraction signal at 19.4°, corresponding to the second peak of the fullerene, is weakly visible but has a similar intensity and shape for both P3HT:PCBM and P3HT:bis-PCBM. In contrast to the blends with Si-PCPDTBT, the XRD results do not give any evidence to support that the overall ordering and crystallization of P3HT:PCBM films is varied by replacing PCBM with bis-PCBM. This observation is in excellent agreement with the solar cell findings for P3HT:PCBM versus P3HT:bis-PCBM devices.

3.4. Electron microscopy and tomography

Fig. 7 shows a conventional bright-field transmission electron microscopy (BF-TEM) image for Si-PCPDTBT:PCBM and Si-PCPDTBT:bis-PCBM photoactive layers. Because of the lower density of the polymer compared with fullerenes, bright regions typically identify polymer-rich phase, where the dark regions indicate fullerene-rich domains [33]. The

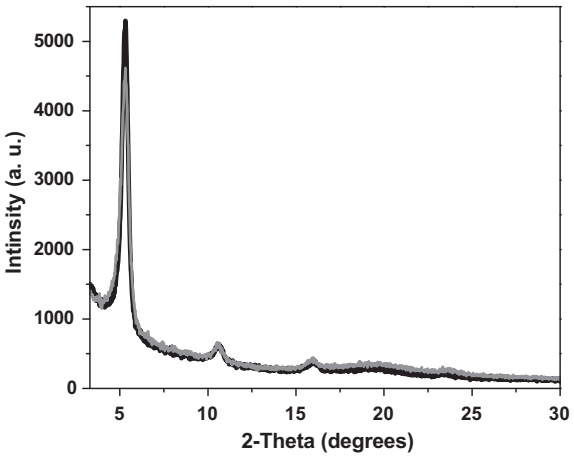

Fig. 6. GIXRD images of films of blend P3HT:bis-PCBM (gray color) and P3HT:PCBM (black color) deposited on quartz substrates and annealed at 140 °C for 5 min.

blend of polymer Si-PCPDTBT with PCBM is found to form a highly functional nanomorphology with the domain size of 10–20 nm, which ensures the efficient excitons separation and collection [15]. TEM images show that bis-PCBM forms finer network in the blend with the polymer Si-PCPDTBT. The transport of the hole and electron through each phase is strongly influenced by the local order and crystallinity within each phase and in addition to the size of domains. The current findings agree with the measured low electrons and holes mobility for Si-PCPDTBT:bis-PCBM devices [17]. A too fine morphology disturbs the continuous percolation pathways required for an efficient charge transport. In P3HT:PCBM based solar cells, the gain in solar cell efficiency is achieved by improved crystallization as well as optimized phase segregation after post-thermal annealing [34,35].

Furthermore, TEM images show some elongated bright features, with characteristic diameter in the few tens of nanometers, which represent polymer nanofibers. These are more evident in blends with PCBM (Fig. 7a). In both images of Fig. 7 some white spots can be seen that represent thinner areas of the samples under investigation. The presence of such thinner parts might be an indication for dewetting of the photoactive layer when deposing it on the PEDOT:PSS substrate.

Conventional BF-TEM images are two-dimensional (2D) projections of the actual 3D sample; therefore they cannot clearly represent bulk features with size much smaller than the sample thickness, due to the overlapping of individual projections. In order to overcome this limitation, electron tomography (ET) was used to perform 3D imaging of nanostructure of the polymer:fullerene composites [36–38]. This method has been recently utilized in OPVs with a resolution in the range of 5–20 nm, which matches well with the dimension of the phase separated domains [39–42]. Fig. 8 shows a few images extracted from reconstructed tomograms (using the SIRT algorithm) of Si-PCPDBT:PCBM and Si-PCPDBT:bis-PCBM photoactive layers at different locations across the film thickness. For the samples we assign bottom, middle and top part of the film as referring to the interface of the sample in contact with the bottom PEDOT:PSS/ITO electrode, the central part of the photoactive layer and the top surface, respectively. The bottom images of both samples show indications of an originally rough interface with PEDOT:PSS. In particularly the white areas in the image of the Si-PCPDTBT:bis-PCBM sample may point to dewetting as already introduced when discussing the conventional BF-TEM images. The fuzzy areas of both images are reconstruction artifacts resulting mainly from the missing wedge; i.e. the limited tilting angle during tomographic tilt-series acquisition.

Approaching the middle region of the Si-PCPDTBT:PCBM layer, a considerable number of uniformly distributed polymer nanofibers are observed, extending all through the film up to the upper region. Similarly, fibers can be observed also across significant parts of the Si-PCPDBT:bis-PCBM film, with an increase in density in the upper part of the bis-fullerene blend film. In case of bis-PCBM, one can see slightly higher densification of polymer fibers at the top of the film. The polymer enrichment near top of the film, i.e. at the electron extracting interface, is of course unfavorable. The origin of fiber formation has been previously discussed in other systems and relates in part to the drying kinetics of the film

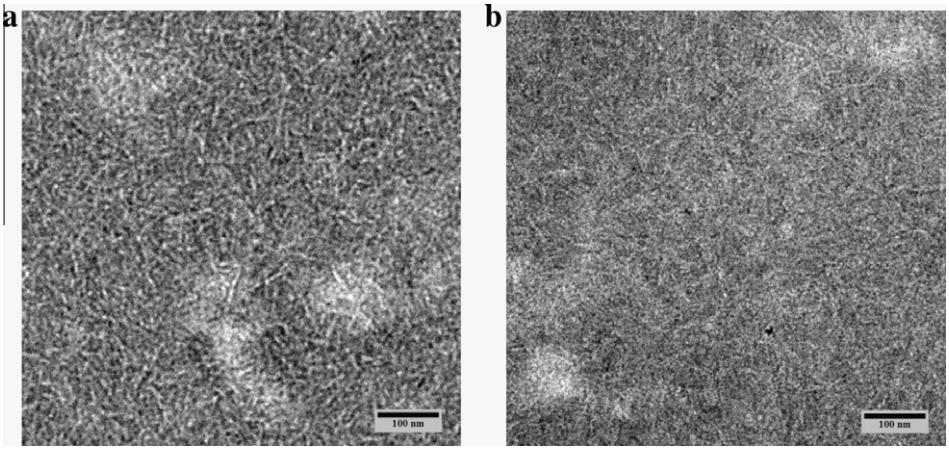

Fig. 7. Bright-field TEM images of blend films doctor-bladed from ODCB: (a) Si-PCPDTBT:PCBM and (b) Si-PCPDTBT:bis-PCBM. The scale bar is 100 nm.

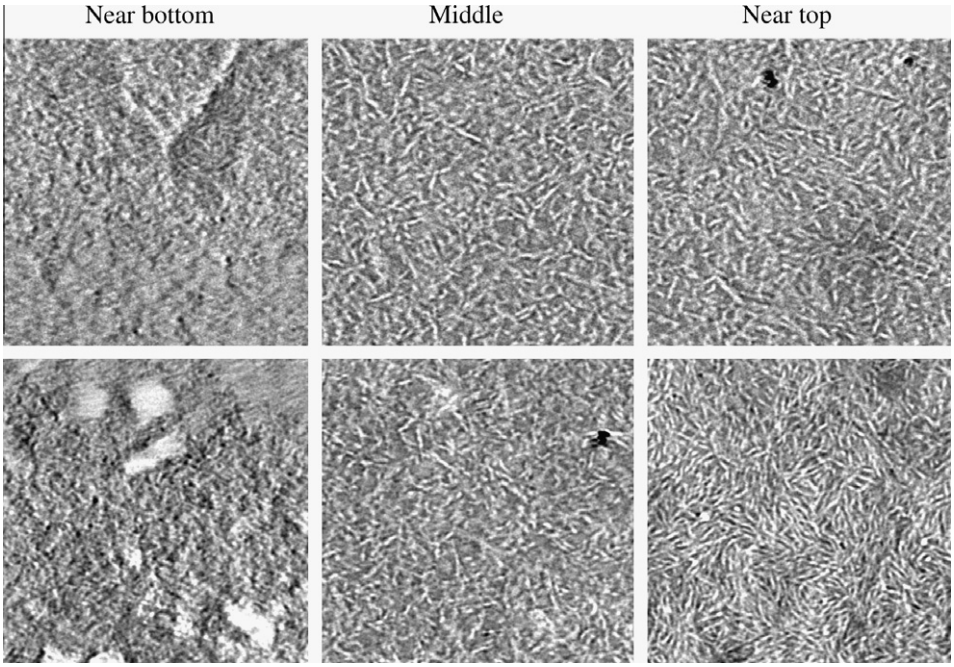

Fig. 8. Electron tomography images for the active layers of Si-PCPDTBT:PCBM (top three images) and Si-PCPDTBT:bis-PCBM (bottom image raw).The image size is in either case around 1.08 μm. The captured slices lie in the horizontal (*X*, *Y*) plane of the film at a different depths (*Z* location): one slice close to the top of the film (the free surface of the film), another one in the middle of the film, and the third one close to the bottom of the film (the one on the copper grid substrate side).

[40]. For films prepared in a similar way, the most relevant difference between the two systems is the significant gap in solubility between bis-PCBM over PCBM that we have observed. In ortho-dichlorobenzene (ODCB), here used for the device and sample preparation, we found the average solubility of 13.68 wt% for bis-PCBM and about 4.58 wt% for PCBM (see the appendix for details of the solubility test). The solubility of fullerene is an important factor that influences the domain formation and crystallization. The small phase segregated domains of Si-PCPDTBT:bis-PCBM correlates with the higher solubility of bis-fullerene that allows the composite to self-organize in a more intimate mixture. The presented results show the close correlation between the thin film microstructure and device performance of oBHJ solar cells.

4. Conclusions

In conclusion, the microstructure of Si-PCPDTBT:PCBM versus Si-PCPDTBT:bis-PCBM thin films and solar cell devices was investigated by various experimental methods. The observation of a glass transition and absence of a melting peak suggest that bis-PCBM is more amorphous than PCBM. This conclusion is also supported by XRD measurements. The morphological differences between PCBM and bis-PCBM are however dependent on the host polymer. In RR-P3HT blends, XRD studies show no evident differences in the fullerene arrangement by exchanging PCBM with bis-PCBM. This is different for Si-PCPDTBT where films with bis-PCBM showed lower crystallinity compared to those with PCBM. As a consequence of better intermixing, TEM results show the fine phase-separated domain sizes of Si-PCPDTBT:bis-PCBM film. Overall, we conclude that the replacement of mono-PCBM by bis-PCBM leads to more disturbed microstructure between the polymer and the fullerene. This more unfavorable microstructure is responsible for the worse transport properties of the blends. The results presented here on the nano-structure of blends offer fundamental information to interpret the peculiar behavior of solar cells based on Si-PCPDTBT:bis-PCBM.

Acknowledgements

We acknowledge the financial support of the Christian Doppler Laboratory for Surface Optics.

Appendix A. Supplementary data

Supplementary data associated with this article can be found, in the online version, at http://dx.doi.org/10.1016/j.orgel.2012.03.031.

References

[1] J. Li, N. Sun, Z.-X. Guo, C. Li, Y. Li, L. Dai, D. Zhu, D. Sun, Y. Cao, L. Fan, J. Phys. Chem. B 106 (2002) 11509–11514.
[2] C.L. Chochos, S.P. Economopoulos, V. Deimede, V.G. Gregoriou, M.T. Lloyd, G.G. Malliaras, J.K. Kallitsis, J. Phys. Chem. C 111 (2007) 10732–10740.
[3] F.B. Kooistra, J. Knol, F. Kastenberg, L.M. Popescu, W.J.H. Verhees, J.M. Kroon, J.C. Hummelen, Org. Lett. 9 (2007) 551–554.
[4] R.Y.C. Shin, T. Kietzke, S. Sudhakar, A. Dodabalapur, Z.-K. Chen, A. Sellinger, Chem. Mater. 19 (2007) 1892–1894.
[5] C. Yang, J.Y. Kim, S. Cho, J.K. Lee, A.J. Heeger, F. Wudl, J. Am. Chem. Soc. 130 (2008) 6444–6450.

[6] P. a Troshin, H. Hoppe, J. Renz, M. Egginger, J.Y. Mayorova, A.E. Goryachev, A.S. Peregudov, R.N. Lyubovskaya, G. Gobsch, N.S. Sariciftci, V.F. Razumov, Adv. Funct. Mater. 19 (2009) 779–788.
[7] R.B. Ross, C.M. Cardona, D.M. Guldi, S.G. Sankaranarayanan, M.O. Reese, N. Kopidakis, J. Peet, B. Walker, G.C. Bazan, E. Van Keuren, B.C. Holloway, M. Drees, Nat. Mater. 8 (2009) 208–212.
[8] Y. He, H.-Y. Chen, J. Hou, Y. Li, J. Am. Chem. Soc. 132 (2010) 1377–1382.
[9] M. Lenes, G.-J.aH. Wetzelaer, F.B. Kooistra, S.C. Veenstra, J.C. Hummelen, P.W.M. Blom, Adv. Mater. 20 (2008) 2116–2119.
[10] D. Jarzab, F. Cordella, M. Lenes, F.B. Kooistra, P.W.M. Blom, J.C. Hummelen, M. a Loi, J. Phys. Chem. B 113 (2009) 16513–16517.
[11] M. Lenes, S.W. Shelton, A.B. Sieval, D.F. Kronholm, J.C. Hummelen, P.W.M. Blom, Adv. Funct. Mater. 19 (2009) 3002–3007.
[12] J. Peet, J.Y. Kim, N.E. Coates, W.L. Ma, D. Moses, a J. Heeger, G.C. Bazan, Nat. Mater. 6 (2007) 497–500.
[13] J. Hou, H.-Y. Chen, S. Zhang, G. Li, Y. Yang, J. Am. Chem. Soc. 48 (16) (2008) 145.
[14] M.C. Scharber, M. Koppe, J. Gao, F. Cordella, M. a Loi, P. Denk, M. Morana, H.-J. Egelhaaf, K. Forberich, G. Dennler, R. Gaudiana, D. Waller, Z. Zhu, X. Shi, C.J. Brabec, Adv. Mater. 22 (2010) 367–370.
[15] M. Morana, H. Azimi, G. Dennler, H.-J. Egelhaaf, M. Scharber, K. Forberich, J. Hauch, R. Gaudiana, D. Waller, Z. Zhu, K. Hingerl, S.S. van Bavel, J. Loos, C.J. Brabec, Adv. Funct. Mater. 20 (2010) 1180–1188.
[16] H. Azimi, M. Morana, T. Ameri, B. Dastmalchi, M. Scharber, K. Hingerl, C.J. Brabec, Sol. Energy Mater. Sol. Cells 95 (2011) 3093–3098.
[17] H. Azimi, A. Senes, M. Scharber, K. Hingerl, C.J. Brabec, Adv. Energy Mater. 1 (2011) 1162–1168.
[18] R. Gaudiana, R. Kingsboraugh, X. Shi, D. Waller, Z. Zhu, US patent 2008 087 324, 2008.
[19] T. Ameri, G. Dennler, C. Waldauf, P. Denk, K. Forberich, M.C. Scharber, C.J. Brabec, K. Hingerl, J. Appl. Phys. 103 (084) (2008) 506.
[20] C. Waldauf, M. Morana, P. Denk, P. Schilinsky, K. Coakley, S.A. Choulis, C.J. Brabec, Appl. Phys. Lett. 89 (2006) 233517.
[21] A.L. Patterson, Phys. Rev. 56 (1939) 978–982.
[22] S. Bertho, I. Haeldermans, A. Swinnen, W. Moons, T. Martens, L. Lutsen, D. Vanderzande, J. Manca, A. Senes, A. Bonfiglio, Sol. Energy Mater. Sol. Cells 91 (2007) 385–389.
[23] C. Müller, T.aM. Ferenczi, M. Campoy-Quiles, J.M. Frost, D.D.C. Bradley, P. Smith, N. Stingelin-Stutzmann, J. Nelson, Adv. Mater. 20 (2008) 3510–3515.
[24] A.M. Ballantyne, T.aM. Ferenczi, M. Campoy-Quiles, T.M. Clarke, A. Maurano, K.H. Wong, W. Zhang, N. Stingelin-Stutzmann, J.-S. Kim, D.D.C. Bradley, J.R. Durrant, I. McCulloch, M. Heeney, J. Nelson, S. Tierney, W. Duffy, C. Mueller, P. Smith, Macromolecules 43 (2010) 1169–1174.
[25] Y. Kim, S. a Choulis, J. Nelson, D.D.C. Bradley, S. Cook, J.R. Durrant, Appl. Phys. Lett. 86 (2005) 063502.
[26] M. Reading, D.J. Hourston (Eds.), Modulated Temperature Differential Scanning Calorimetry: Theoretical and Practical Applications in Polymer Characterisation, Springer, Dordrecht, 2006.
[27] J. Zhao, A. Swinnen, G. Van Assche, J. Manca, D. Vanderzande, B. Van Mele, J. Phys. Chem. B 113 (2009) 1587–1591.
[28] J.-H. Tsai, Y.-C. Lai, T. Higashihara, C.-J. Lin, M. Ueda, W.-C. Chen, Macromolecules 43 (2010) 6085–6091.
[29] Y. Zhang, H.-L. Yip, O. Acton, S.K. Hau, F. Huang, A.K.-Y. Jen, Chem. Mater. 21 (2009) 2598–2600.
[30] M.L. Chabinyc, Polym. Rev. 48 (2008) 463.
[31] T. Erb, U. Zhkavhets, G. Godch, S. Raleva, B. Stuhn, P. Schilinsky, C. Waldauf, C.J. Brabec, Adv. Funct. Mater. 15 (2005) 1193.
[32] M. Reyes-Reyes, R. López-Sandoval, J. Arenas-Alatorre, R. Garibay-Alonso, D.L. Carroll, A. Lastras-Martinez, Thin Solid Films 516 (2007) 52–57.
[33] C.W.T. Bulle-Lieuwma, W.J.H. van Gennip, J.K.J. van Duren, P. Jonkheijm, R.A.J. Janssen, J.W. Niemantsverdriet, Appl. Surf. Sci. 547 (2003) 203–204.
[34] C.J. Brabec, M. Heeney, I. McCulloch, J. Nelson, Chem. Soc. Rev. 40 (2011) 1185–1199.
[35] D. Chirvase, J. Parisi, J.C. Hummelen, V. Dyakonov, Nanotechnology 15 (2004) 1317–1323.
[36] P. a Midgley, R.E. Dunin-Borkowski, Nat. Mater. 8 (2009) 271–280.
[37] H. Friedrich, P.E. de Jongh, A.J. Verkleij, K.P. de Jong, Chem. Rev. 109 (2009) 1613–1629.
[38] P. a Midgley, M. Weyland, Ultramicroscopy 96 (2003) 413–431.
[39] S.D. Oosterhout, M.M. Wienk, S.S. van Bavel, R. Thiedmann, L.J.A. Koster, J. Gilot, J. Loos, V. Schmidt, R.A.J. Janssen, Nat. Mater. 8 (2009) 818–824.
[40] S.S. van-Bavel, E. Sourty, G. de With, J. Loos, Nano Lett. 9 (2009) 507–513.
[41] B.V. Andersson, A. Herland, S. Masich, O. Inganäs, Nano Lett. 9 (2009) 853–855.
[42] A.A. Herzing, L.J. Richter, I.M. Anderson, J. Phys. Chem. C 114 (2010) 17501–17508.